Hindawi
Geofluids
Volume 2022, Article ID 4817269, 11 pages
https://doi.org/10.1155/2022/4817269

Research Article

Effect of Amplitude and Confining Pressure on Granite Failure under Ultrahigh Frequency (UHF) Impact Based on Radiation Temperature

Cheng Zhang[1], **Shulei Zhang**[2] **and Dajun Zhao**[1]

[1]*College of Construction Engineering, Jilin University, Changchun 130026, China*
[2]*Yellow River Survey, Planning and Design Institute Co., Ltd., Zhengzhou, Henan 450003, China*

Correspondence should be addressed to Shulei Zhang; zhangshl@yrec.cn and Dajun Zhao; zhaodj@jlu.edu.cn

Received 29 December 2021; Accepted 25 August 2022; Published 20 September 2022

Academic Editor: Basim Abu-Jdayil

Ultrahigh frequency impact technology has great potential to break hard rocks with lower energy consumption. Based on the infrared nondestructive testing technology, the effects of load (i.e., amplitude) and boundary (i.e., confining pressure) conditions on granite damage under ultrahigh frequency impact have been investigated to promote the application of this technology in rock engineering. Experimental results demonstrate that the evolution law of the maximum radiation temperature on granite surface reflects the granite damage state. Under ultrahigh impact, granite specimens are damaged effectively with the impact amplitude exceeding 32 μm, and the failure mode of the specimen is changed by the confining pressure. Depending on Griffith's theory, the extension angle of the fatigue crack changes from 60 to 30 degrees with increasing confining pressure. And the transverse fracture occurs in the upper part of the specimen under ultrahigh frequency impact subjected to confining pressure. This research determines the amplitude threshold of the ultrahigh frequency impact load and verifies the effectiveness of ultrahigh frequency impact technology for granite failure subjected to confining pressure.

1. Introduction

To achieve global carbon neutrality goals, geological resource drilling needs to reduce energy consumption and improve drilling efficiency [1]. Conventional rotary drilling method, breaking rock by mechanical cutting force, has the challenges of low efficiency and high wear rate of drilling tools [2]. The combination of axial impact and rotary cutting is a typical measure to improve the efficiency of rotary drilling [3]. In addition, some novel and unconventional rock breakage methods, including water jet method [4], projectile impact [5], plasma method [6], laser method [7], and a microwave method [8], improve drilling efficiency in hard rock while increasing energy and material utilization. However, limited by the cost of equipment and the drilling environment, these innovation methods have not been applied on a large scale. With the development of an ultrasonic transducer, rotary drilling assisted by axial ultrahigh frequency (UHF) impact has been successfully applied in the field of superhard material processing and is considered an effective method to solve these drilling challenges [9].

For the application of assisted UHF impact technology in drilling engineering, some scholars have designed UHF percussion drills and verified their feasibility of rock breaking under laboratory conditions. Wiercigroch et al. designed a rotary drilling test device assisted by axial UHF impact and conducted drilling tests on hard rocks [10]. Test results show that the assisted UHF impact can significantly increase drilling speed and reduce drilling force. Harkness [11] and Cardoni et al. [12] verified that longitudinal-torsional compound impact can effectively improve rock breaking efficiency. And this technology reduces the weight and wear of the drilling rig, which has high application value in the field of planetary rock drilling and sampling. The above study shows that ultrasonic percussive drills can achieve superior drilling effects under low-power conditions.

However, the mechanism of rock failure is not clear, which limits the application of these drills in practical drilling projects [13, 14].

The frequency of UHF impact is greater than 20 kHz, which is higher than the natural frequency of rock. In solid materials, the propagation of ultrahigh frequency stress wave leads to significant mechanical and thermal effects, which promote material failure [15]. Due to insufficient understanding of rock failure mechanism under UHF impact, some scholars have conducted experimental studies. For rock dynamic mechanical characteristics, through monitoring of the strain evolution on the granite surface, Zhou et al. [16] analyzed the mechanical and damage properties of granite specimens during UHF impact. Experimental results reveal that the deformation of the specimen changes from compression to tension, and the damage starts to occur in tension. In addition, the impact frequency and static force had significant effects on the mechanical properties of granite specimens [17]. Keeping the impact frequency close to the rock natural frequency and selecting the appropriate static force are the key to improving the rock breaking efficiency [18]. Optimal impact frequency and static force in the test are 30 kHz and 200 N, respectively [19]. For rock thermal field evolution, Zhao et al. [20] analyzed the evolution characteristics of the temperature field on the granite surface and established the critical criterion of rock damage based on the temperature variation laws. Moreover, this research reveals that fatigue tensile damage caused by UHF impact and thermal damage caused by high temperature are the primary failure mechanisms of granite [21].

The above studies have established the frequency, static force, and temperature thresholds of granite damage under UHF impact. However, few studies have been conducted on the effect of impact amplitude (i.e., UHF load strength) and confining pressure (i.e., boundary conditions) on granite failure. It is a known fact that load and boundary conditions have a significant influence on the failure process of rocks [22, 23]. The development of rock infrared nondestructive testing technology provides an important method for understanding the mechanism of rock failure under UHF impact. Therefore, based on the infrared NDT technology, the effect of the impact amplitude and the confining pressure on hard rock failure can be investigated.

In this work, the effect of impact amplitude (i.e., 20, 24, 28, 32, 36, and 40 μm) and confining pressure (i.e., 0, 10, and 20 MPa) on granite failure under UHF impact is observed and analyzed using an infrared thermal imaging device. First, based on the maximum temperature curves on the entire UHF impact process, the damage process of the specimen under different impact amplitudes is analyzed. Then, the amplitude threshold for granite strength weakening under the test conditions is determined by uniaxial compressive strength testing. Second, the effect of confining pressure on the failure mode of granite specimens was analyzed by the thermal stress distribution on the rock surface under triaxial UHF impact. And the fatigue crack extension angle of the specimens under triaxial UHF impact is discussed by the Griffith crack extension theory. This research has further perfected the understanding of the rock fracture mechanism under UHF impact and provided theoretical guidance for the practical application of UHF impact.

Table 1: Mineral compositions of granite specimen.

Mineral	Quartz	Feldspar	Biotite	Other minerals
Mineral diameter (mm)	2–3	0.2–0.5	1–2	
Mineral proportion (%)	30–35	50–60	8–10	<1

Table 2: Mechanical parameters of granite specimens.

Density (g/cm^3)	Uniaxial compressive strength (MPa)	Young's modulus (GPa)	Poisson's ratio
2.68 ± 0.03	138.05 ± 19	31.07 ± 12.2	0.29 ± 0.05

2. Methodology of the Experiment

2.1. Sample Preparation. The medium-grain grained cylindrical specimens with a diameter of 35 ± 0.5 mm and a height of 70 ± 0.5 mm were prepared following the International Society Mechanics (ISRM) Standard. The main mineral compositions of granite specimens are shown in Table 1, and the natural physical and mechanical parameters of the specimens are shown in Table 2.

2.2. UHF Impact Test Device. The uniaxial UHF impact test device used in this study is shown in Figure 1(a), consisting of ultrasonic drive power supply, piezoelectric ceramic transducer, ultrasonic horn, tool head, timer, weight, bracket, and granite specimens, which applies impact loads of different amplitudes to granite specimens. The ultrasonic drive power supply converts the frequency of 220 V alternating current from 50 Hz to 30 kHz and outputs it to the ultrasonic generator. The ultrasonic generator consists of a piezoelectric ceramic transducer, ultrasonic horn, and tool head, which generates the ultrahigh frequency impact force. As shown in Figure 2, the piezoelectric ceramic transducer converts the alternating current energy with the frequency of 30 kHz into the ultrahigh frequency mechanical wave energy with the same frequency. Then, the amplitude of the high-frequency mechanical wave is amplified by the ultrasonic horn and transmitted to the tool head. And the tool head obtains the ultrahigh frequency impact force to break the reck samples. By adjusting the power of the ultrasonic drive power supply, which ranges from 0 to ~1200 W, the impact amplitude can be selected from 0 to 40 μm. The weight transfers the static force (200 N) to the tool head through brackets, making the tool head in close contact with the surface of the specimen and improving the transfer efficiency of impact energy.

2.3. Confining Pressure Application Scheme. In order to apply confining pressure to the cylindrical specimen without affecting the UHF impact loading, a simple mechanical device for confining pressure application is designed as shown in Figure 1(b), consisting of a hydraulic pump,

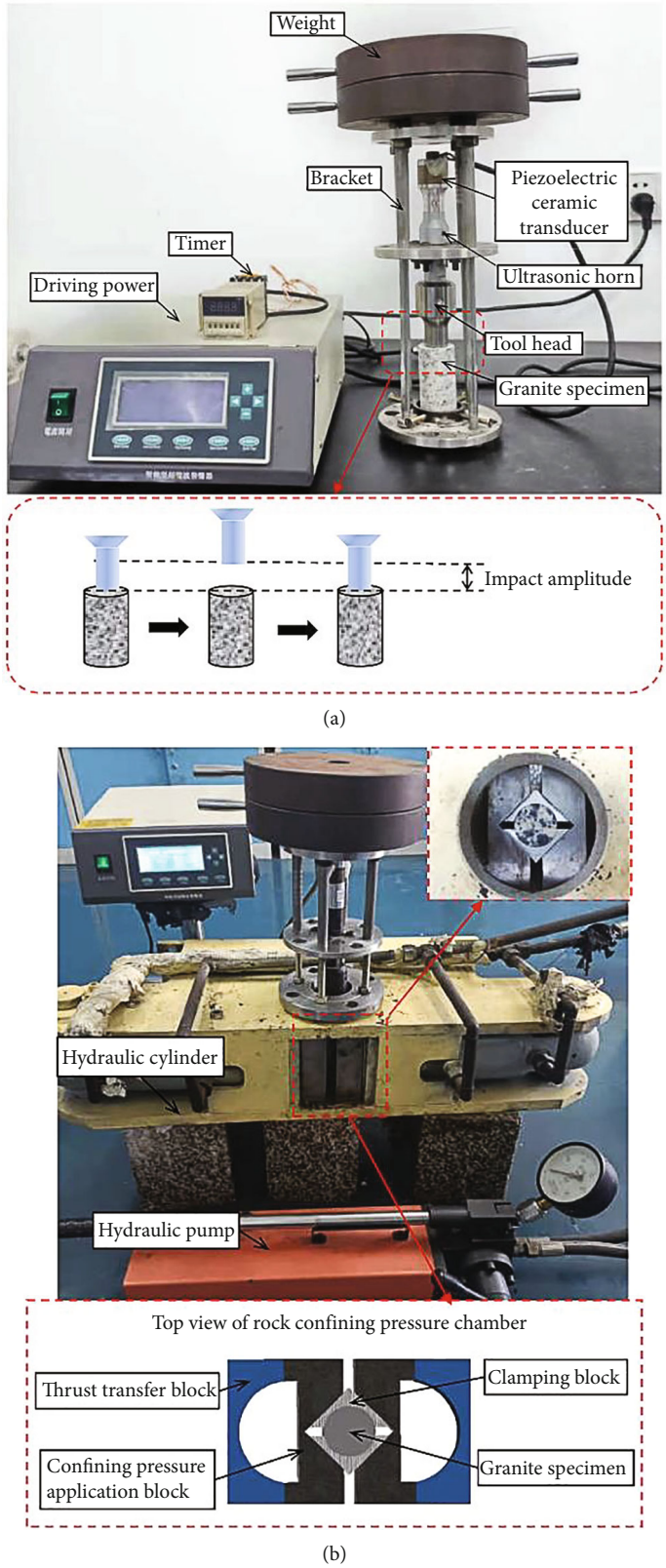

Figure 1: Ultrahigh impact test device: (a) uniaxial ultrahigh impact device; (b) triaxial ultrahigh impact test device.

hydraulic cylinder, thrust transfer block, confining pressure application block, and clamping block. The hydraulic pressure output from the hydraulic pump is converted into a mechanical force by the hydraulic cylinder, and the mechanical force is applied to the thrust transfer block. Then, the confining pressure application block converts the

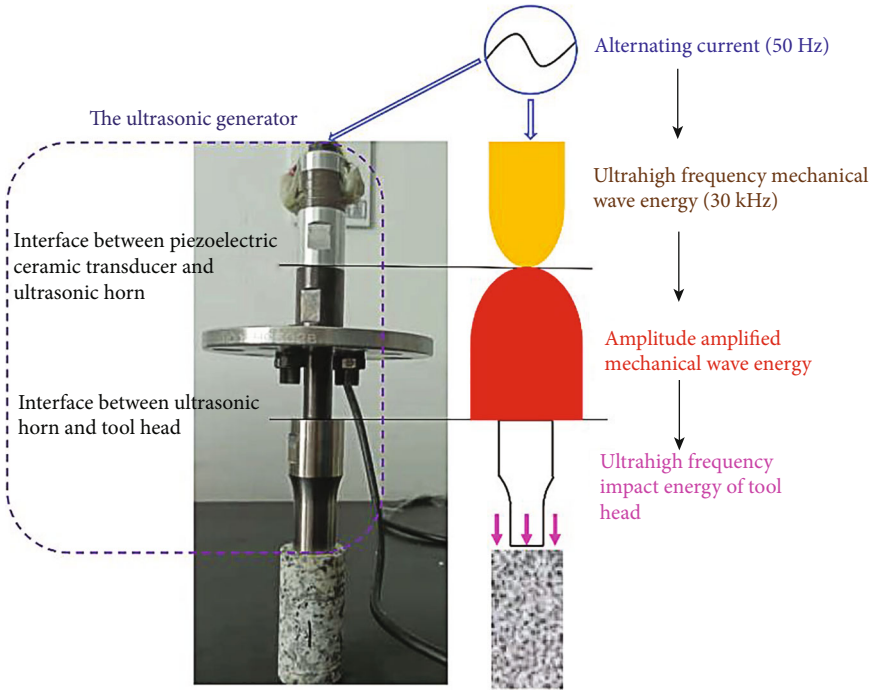

Figure 2: Generation mechanism of ultrahigh frequency impact.

mechanical force transmitted by the thrust transfer block into radial confinement pressure by extrusion deformation. Finally, by the extensional deformation of the clamping blocks, the confining pressure is applied to the side surface of the specimen in a relatively uniform manner.

2.4. Test Procedures. Based on the purpose of the study, the test is conducted into two parts which involved the effect of impact amplitude and confining pressure on granite failure under UHF impact by analyzing the rock surface radiation temperature. Experimental parameters in the tests are as follows: the UHF impact frequency is 30 kHz, the static force is 200 N, and the ultrasonic drive power is 1200 W. Each group contains 3 specimens for repeated tests.

As shown in Figure 3(a), during the entire UHF impact loading with the amplitude of 20, 24, 28, 32, 36, and 40 μm, the infrared radiation temperature of the rock surface was monitored by taking pictures each second through the thermal infrared imager. Each picture contains a matrix of 320×240 pixels, which represents the spatial distribution of infrared radiation temperature values on rock surfaces. By using Textpad software and Tecploct software to process the temperature data, the evolution curve of the radiation temperature with impacts time at each pixel on the rock surface can be obtained. The effect of amplitude on rock damage and fracture under UHF impact can be investigated based on the infrared temperature evolution. Then, the uniaxial compressive strength of granite specimens is measured under UHF impact with different amplitudes for 120 seconds to quantify the degree of rock strength weakening.

As shown in Figure 3(b), only the confining pressure is chosen as the variable to investigate the effect of confining pressure on granite fracture under UHF impact, and the test procedures are as follows: (1) The confining pressure is first applied to the granite specimens slowly, and then, the UHF impact load is applied to the top surface of the specimens for 180 seconds with the impact frequency of 30 kHz, the static force of 200 N, and the impact amplitude of 40 μm. (2) After UHF impact loading, the UHF impact device is immediately removed, and the infrared radiation information of the rock loading surface is measured. (3) Granite specimens were taken out after unloading the confining pressure to observe their fracture model. (4) If there are no macroscopic cracks on the surface of the specimen, the crack dying test is performed on the specimen in the longitudinal section to observe the internal mesodamage of granite.

3. Temperature Criteria for Granite Failure

3.1. Mathematical Relationship between Rock Stress and Infrared Radiation Temperature. The temperature on rock surface changes significantly during rock loading, deformation, and damage, which can be observed by an infrared thermal imager [24]. Several scholars have considered the relationship between the growth of microcracks and the thermal infrared radiation characteristics [25–27]. These studies have shown that the thermoelastic effect and the frictional-thermal effect are the main mechanisms for the generation of thermal radiation on the rock surface, especially for elastic and brittle rocks like granite. And the thermal radiation temperature on the rock surface not only reflects the distribution and intensity of rock internal stress but also reveals the process of rock failure. For rock materials, the mathematical relationship between the infrared radiation temperature on the rock

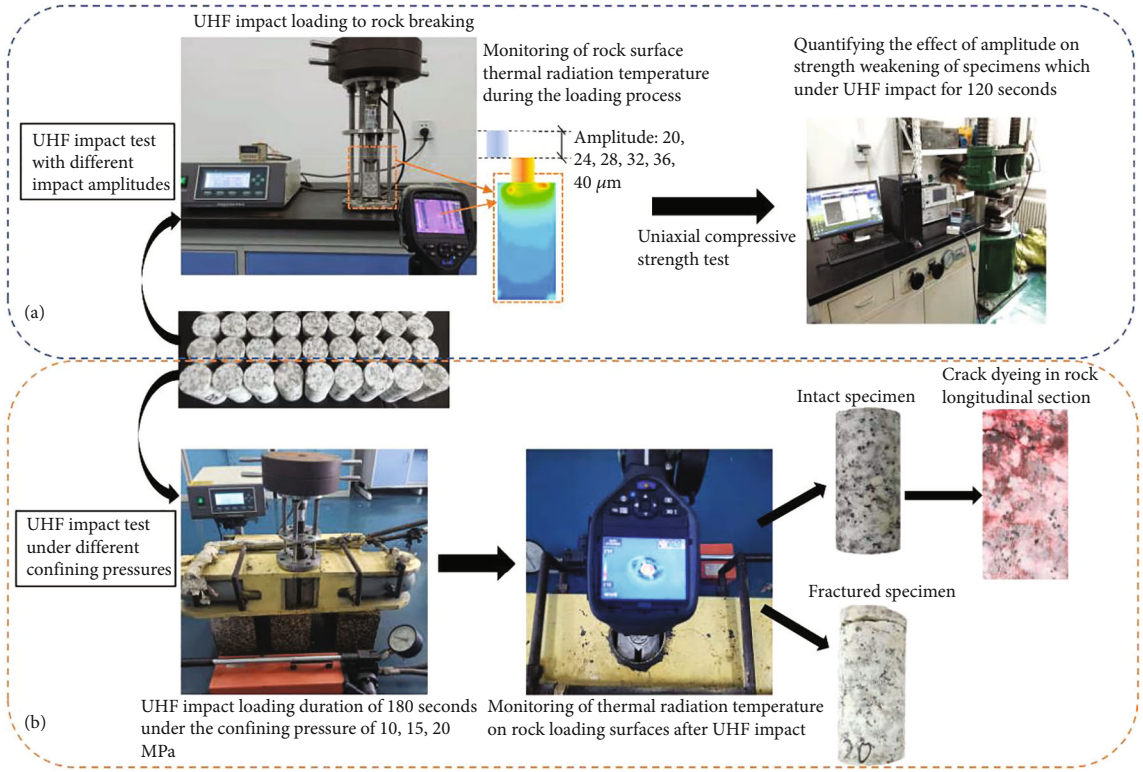

Figure 3: Test procedures: (a) UHF impact test with different impact amplitudes; (b) UHF impact test under different confining pressures.

surface and the internal stress during loading is shown in the following equation [25].

$$\Delta f = \gamma \beta^{-1} T \Delta(\sigma_1 + \sigma_2), \tag{1}$$

where Δf (K) is the increment of rock surface infrared radiation temperature, T is the absolute temperature of the loaded rock, β (K) is the parameter correction factor, and γ (KU^{-1}) is the signal conversion factor.

Equation (1) shows that the increment of infrared radiation temperature on the rock surface is proportional to the sum of the principal stresses. Without the frictional heat and heat dissipation due to the rock damage, the infrared radiation temperature on the rock surface would increase steadily with loading time and principal stress. That is, the failure process of the rock can be analyzed through the erratic fluctuations in the infrared radiation temperature.

3.2. Maximum Temperature Criteria for Rock Failure. The evolution laws of the maximum, average, and minimum temperatures on the rock surface are the important indicators in remote sensing rock mechanics [28]. Figure 4 shows the curves of temperature (i.e., maximum, average, and minimum temperature) on granite surface with loading time under UHF impact. The results demonstrate that only the maximum temperature curve exhibits typical stage-change characteristics (i.e., temperature grows linearly in stage I, temperature rises sharply in stage II, and temperature fluctuates rapidly in stage III) with the development of granite failure. Under different loading conditions, as microcracks emerge and expand in the rock, anomalous changes of infrared radiation temperatures on the rock surface include transient rising, rapidly falling, and first decreasing and then increasing [29]. In stage I, during the elastic deformation, the thermoelastic effect causes a linear increase in elastic heat with loading time. The UHF impact load has not effectively damaged the rock, and the primary microcracks inside the rock remain closed at this stage. In stage II, after the ending of the elastic deformation, the emergence and growth of microcracks generate a large amount of frictional heat, leading to a sharp rise in rock surface temperature. In stage III, under the continuous UHF impact, the generation of macroscopic fractures leads to an enormous amount of energy dissipation which makes the temperature fluctuate dramatically. In summary, these variations in maximum infrared radiation temperature reveal the damage stage of rock under UHF impact.

4. Amplitude Thresholds for Granite Damage under UHF Impact

4.1. Maximum Temperature Evolution under UHF Impact with Different Amplitudes. Figure 5 shows the maximum-time curves during full UHF impact with the amplitude of 20, 24, 28, 32, 36, and 40 μm. The results show that the maximum temperature curves exhibit the variation characteristics similar to those in Figure 4 at the amplitude of 32, 36, and 40 μm, which reveals the emergence and extension of microcracks and the occurrence of a local macroscopic fracture inside granite specimens. In addition, as the impact amplitude increases, the shorter the elastic deformation

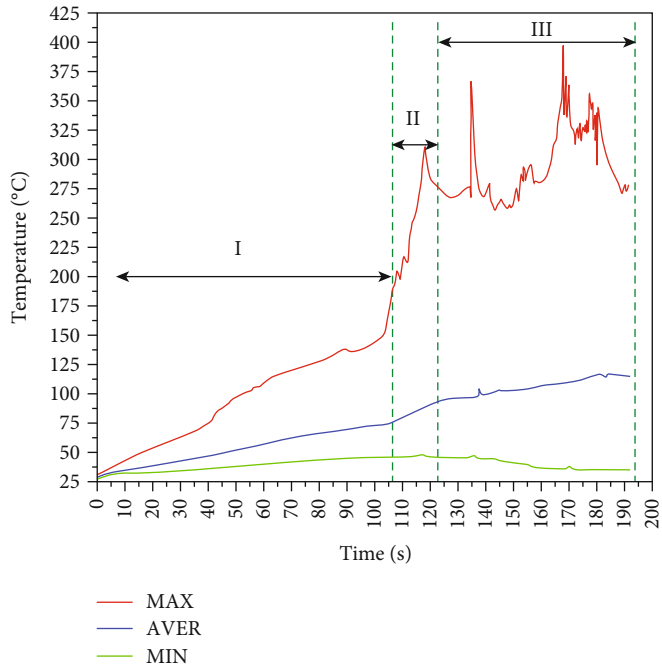

Figure 4: MAM temperature-time curves.

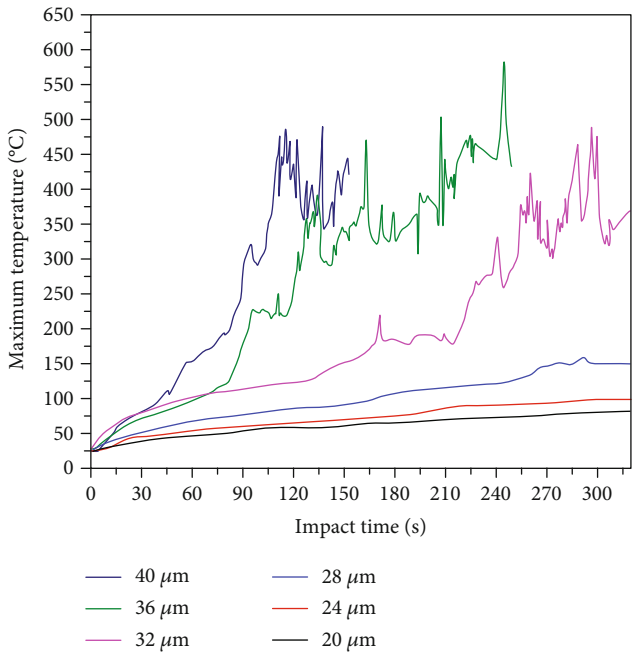

Figure 5: Maximum temperature-time curves under UHF impact with different impact amplitudes.

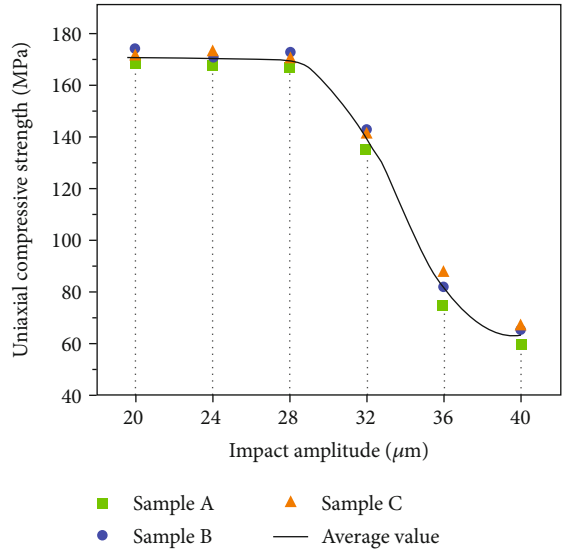

Figure 6: Uniaxial compressive strength of granite specimens under 120 seconds of UHF impact with different amplitudes.

phase is, the faster the rock damage and fracture appearance. When the value of the impact amplitude is 20, 24, and 28 μm, the maximum temperature curve changes smoothly, indicating elastic deformation of rock.

4.2. Effect of Amplitude on Granite Strength Weakening under 120 Seconds of UHF Impact. Figure 6 shows the effect of the impact amplitude on granite strength weakening under the same duration of UHF impact, which quantitatively verifies the effect of amplitude on rock failure. The test results indicate that the uniaxial compressive strength of granite decreases significantly when the impact amplitude reaches 32, 36, and 40 μm. And the compressive strength weakens to 60 MPa at 40 μm, which is only one-third of the strength at the amplitude of 28 μm. In contrast, the compressive strength of the specimens is maintained around 170 MPa at the amplitude of 20, 24, and 28 μm. In summary, significant damage occurs when the impact amplitude exceeds 32 μm, and the fracture efficiency of rock under UHF impact increases with the increasing amplitude. Under

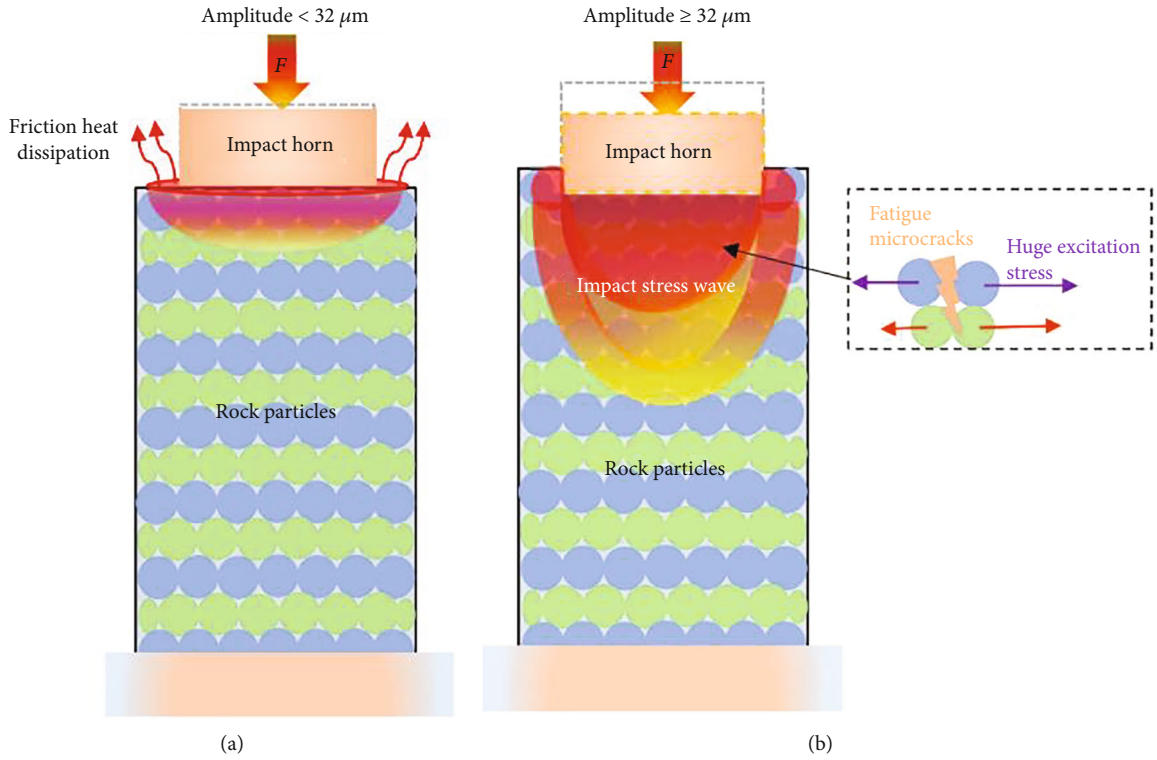

Figure 7: Effect of amplitude on the propagation of load stress wave: (a) amplitude < 32 μm; (b) amplitude ≥ 32 μm.

the present test conditions, the optimal amplitude value for the granite fracture is 40 μm.

4.3. Theoretical Analysis of Granite Fracture under UHF Impact with Different Amplitudes. The UHF impact load applied to the granite specimens is shown in the following equation.

$$F = A \sin 2\pi f t, \tag{2}$$

where A is the amplitude of the UHF impact load, f is the UHF impact frequency, and t is the impact time.

Different from conventional impact loads (i.e., the frequency usually less than 100 Hz), the UHF impact load has a super-higher impact frequency (i.e., usually greater than 20 kHz) and the smaller amplitude (i.e., usually less than 60 μm), which results in a different rock fracture mechanism. Although the value of the UHF impact load is low, rock particles within a certain range can obtain an extremely high acceleration. As shown in Equation (3) [21], a is the acceleration of rock particles, which are 10^6 times of that under conventional impact loads. According to Newton's second law, huge excitation forces are generated between rock particles, resulting in fatigue damage.

$$a = -A4\pi^2 f^2 \sin 2\pi f t. \tag{3}$$

Figure 7 illustrates the effect of amplitude on the propagation of the load stress wave. The UHF impact load stress wave is not sufficient to propagate in the granite specimen when the amplitude is small, which places the granite specimen in a state of static compression. And load energy is dissipated in the form frictional heat which resulted from the friction between the horn and the granite surface. When the amplitude exceeds 32 μm, the UHF impact load stress wave is sufficient to propagate in the granite specimen, resulting in huge excitation stress between rock particles and leading to fatigue failure.

5. Effect of Confining Pressure on Granite Failure under UHF Impact

5.1. Failure Modes of Granite Subjected to Different Confining Pressures. Based on the above study of amplitude, the optimal amplitude of 40 μm was chosen for the subsequent experiment. Figure 8 shows the failure modes of granite specimens under UHF impact subjected to the confining pressures of 0, 10, and 20 MPa. Under the UHF impact for 180 seconds, upper splitting occurs at the confining pressure of 0 MPa, and mesodamage occurs at the confining pressure of 10 MPa without any macrocracks on the rock surface, and transverse fracture occurs at the confining pressure of 20 MPa. Numerous studies have indicated that confining pressure increases the strength of rock and inhibits the generation of macrofractures [30–33]. Therefore, under the confining pressure of 10 MPa, the extension and penetration of microcracks in the specimen are significantly inhibited by the confining pressure, which is the reason for the integrity of the specimen. Comparing to the failure mode at the

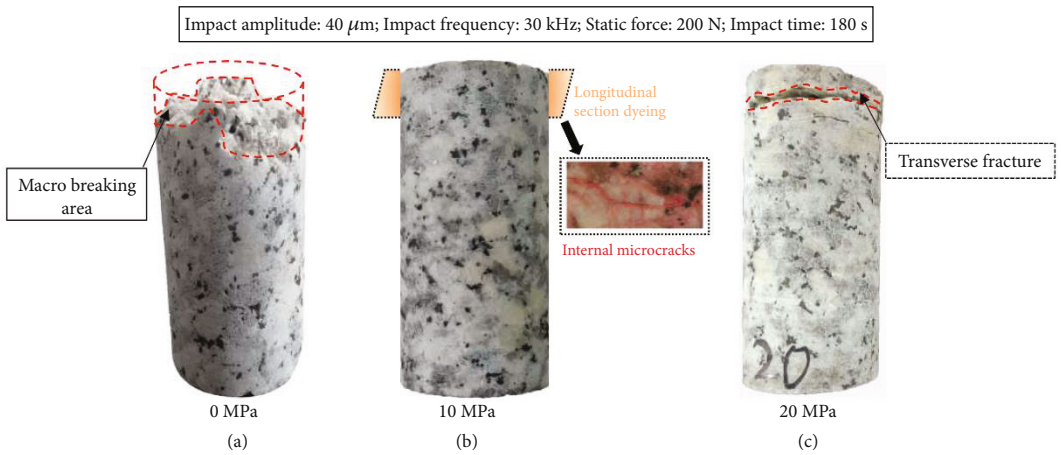

Figure 8: Granite failure modes under UHF impact subjected to confining pressure: (a) confining pressure of 0 MPa; (b) confining pressure of 10 MPa; (c) confining pressure of 20 MPa.

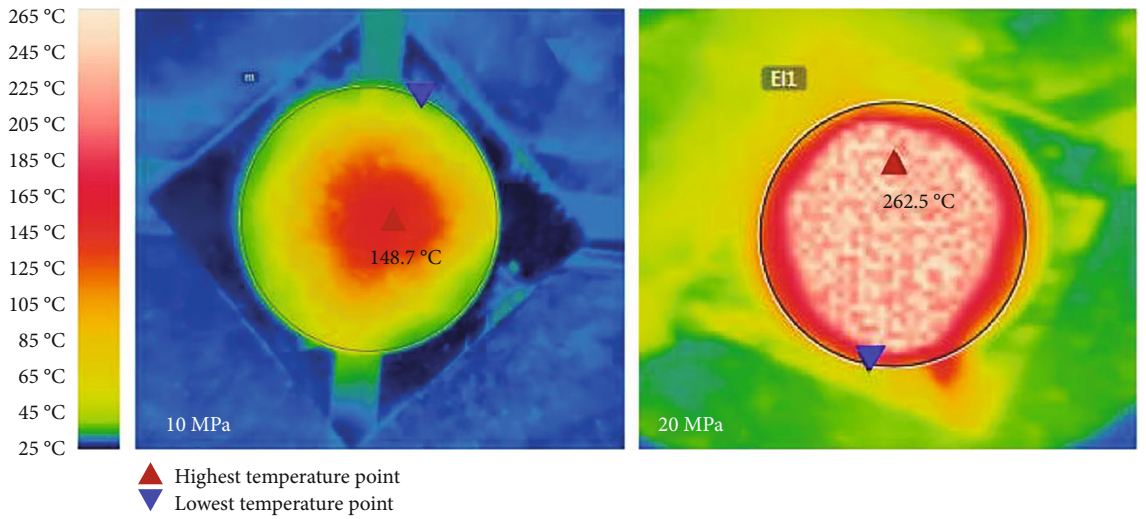

Figure 9: Infrared thermal radiation distribution on granite loading surface after UHF impact subjected to the confining pressure of 10 and 20 MPa.

confining pressure of 0 MPa, significant difference occurred at the confining pressure of 20 MPa, which deserves further discussion.

5.2. Analysis of Granite Failure Mode under UHF Impact Subjected to Confining Pressure. Figure 9 reflects the distribution and intensity of infrared thermal radiation (i.e., internal stress) on the loading surface under UHF impact subjected to the confining pressure of 10 and 20 MPa. Under the confining pressure of 10 MPa, the infrared radiation temperature decays radially from the center of the loading surface towards the edges, and the specimen remains intact with mesodamage after UHF impact. Under the confining pressure of 20 MPa, the penetration of transverse fracture causes a large release of loading energy along the fracture plane, which expands the range of the maximum infrared radiation temperature on the loading surface. And the maximum radiation temperature increases by nearly 110°C with the 10 MPa increment of the confining pressure.

The characteristics of infrared radiation temperature are positively correlated with the rock stress state, which reveals the generation mechanism of the transverse fracture of the specimen under the UHF impact subjected to the confining pressure. As shown in Figures 10(a) and 10(b), the ring-shaped compression zone is formed at the edge of the specimen, restraining the macroscopic fracture of the specimen surface, under the combined compression of the central thermal expansion stress and confining pressure. Under the UHF impact, the thermal stress in the longitudinal section of the specimen is mainly concentrated within 10 mm from the loading surface (Figure 10(b)). As a result, this part of the rock is more compact and less fragile, which leads the shear penetration occurring at 10~15 mm from the loading surface and the upper fragment remaining intact (Figure 10(c)). As shown in Figure 8, the depth of the transverse fracture is consistent with the effective fatigue breaking depth under the uniaxial UHF impact; thus, the transverse fracture is formed by secondary shear penetration of fatigue tensile cracks.

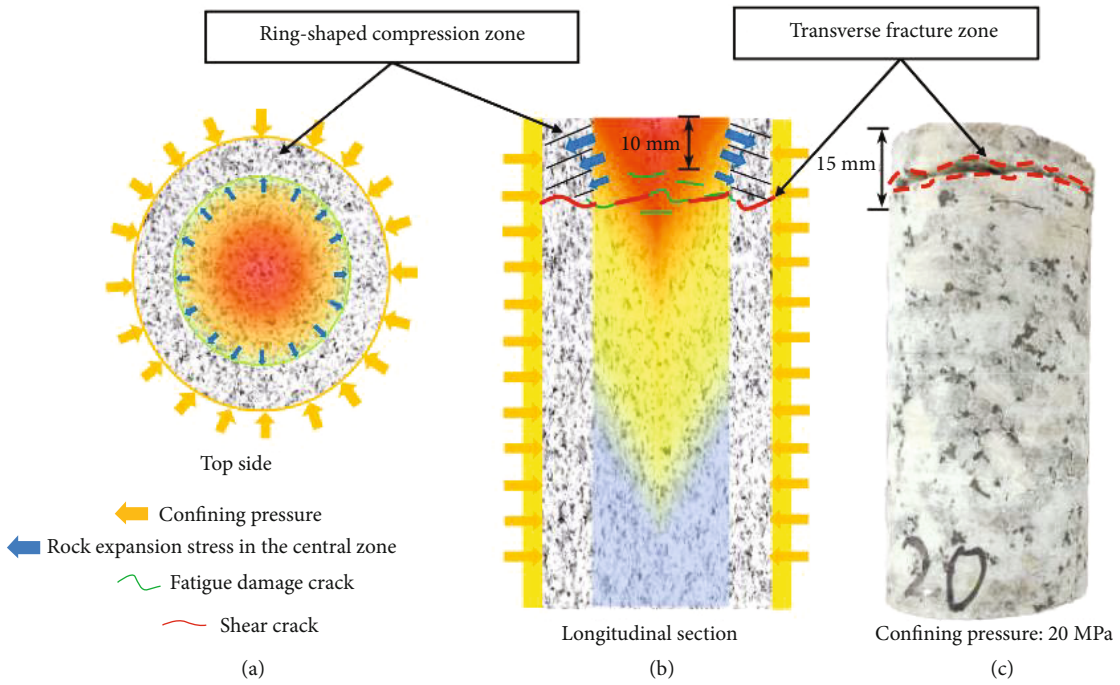

Figure 10: Rock stress distribution states and failure development under UHF impact subjected to confining pressure: (a) stress distribution on granite loading surface; (b) stress distribution and damage development on granite longitudinal section; (c) fracture model of granite under UHF impact subject to the confining pressure of 20 MPa.

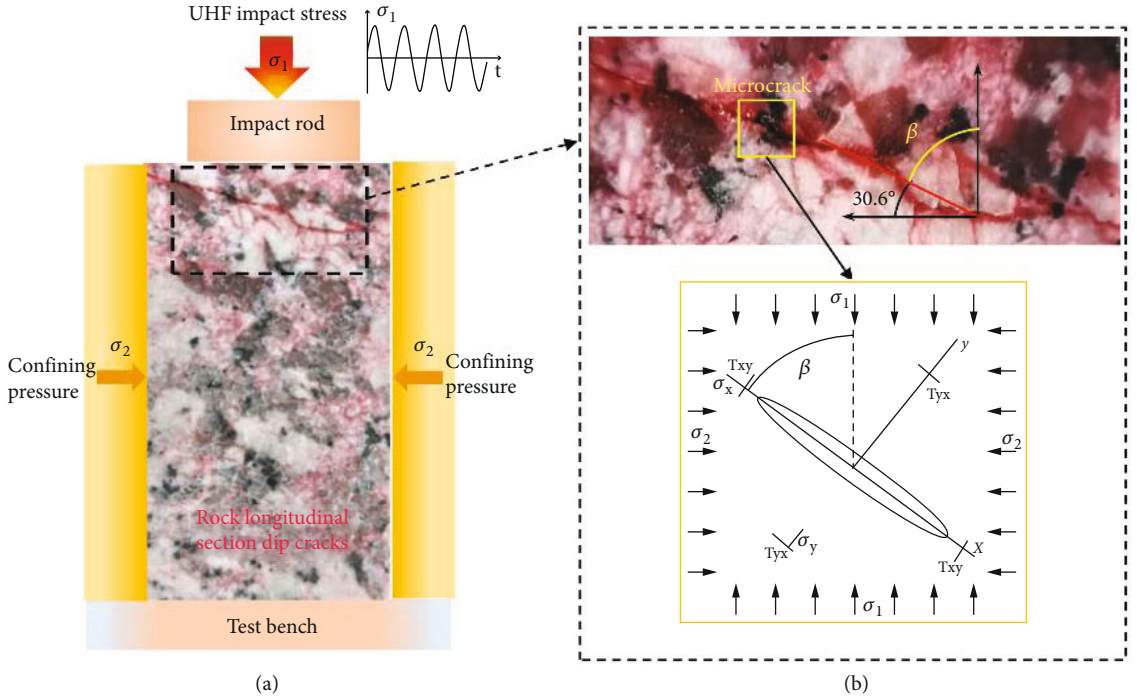

Figure 11: Microcrack extension angle model for granite after UHF impact: (a) microcrack dipping in longitudinal sections of granite; (b) microcrack extension angle and Griffith crack extension model.

Figure 11 shows the fatigue crack extension model inside granite under UHF impact and reveals that the crack extension angle is in accordance with the Griffith strength theory. The UHF impact tress σ_1 is shown in the following equation [14].

$$\sigma_1 = -\Delta m A 4\pi^2 f^2 \sin(2\pi f t), \tag{4}$$

where Δm is the mass of unit particles, A is the impact amplitude, and f is the impact frequency.

According to the Griffith crack stress model in Figure 11(b), the fatigue crack extension azimuth angle β inside rock can be expressed by the following equation.

$$\beta = 0, \quad \begin{pmatrix} \sigma_1 > 0, \sigma_2 < 0, \sigma_1 + 3\sigma_2 < 0 \\ \sigma_1 < 0, \sigma_2 < 0, \sigma_1 + 3\sigma_2 < 0 \end{pmatrix},$$
$$\cos 2\beta = \frac{\sigma_1 - \sigma_2}{2(\sigma_1 + \sigma_2)}, \quad \begin{pmatrix} \sigma_1 > 0, \sigma_2 > 0, \sigma_1 + 3\sigma_2 > 0 \\ \sigma_1 > 0, \sigma_2 < 0, \sigma_1 + 3\sigma_2 > 0 \end{pmatrix}, \quad (5)$$
$$\beta = \frac{\pi}{2}, \quad (\text{except for the above two cases}).$$

When the confining pressure σ_2 is 10 MPa, the stress of granite satisfies $\sigma_2 \gg \sigma_1$, and the maximum principal stress direction is parallel to the confining pressure σ_2. Based on the rule that compression is positive and tensile is negative, the UHF impact stress σ_1 and the confining pressure σ_2 are considered to be positive, as shown in Figure 11(a). Therefore, the fatigue crack extension azimuth angle is consistent with that $\cos 2\beta = \sigma_1 - \sigma_2/2(\sigma_1 + \sigma_2) \approx -1/2$; that is, the crack extends at an angle of 30 degrees (i.e., $\beta = \pi/3$) as shown in Figure 10(b). When the stress of granite satisfies $\sigma_1 > \sigma_2$, the crack extension angle should be less than 60 degrees (i.e., $\beta > \pi/6$). In summary, the extension angle of the fatigue crack under UHF impact subjected to confining pressure should range between 30 and 60 degrees.

6. Conclusion

Based on the infrared radiation temperature characteristics, this research first investigated the amplitude threshold (i.e., loading parameter) of granite failure under UHF impact and then analyzed the effect of confining pressure (i.e., boundary conditions) on the granite macroscopic fracture mode and fatigue crack extension angle. The test results verify the efficiency of the UHF impact load in breaking granite subjected to confining pressure. Compared to existing researches, the amplitude threshold for granite effective breaking was determined, and the impact amplitude and confining pressure were considered simultaneously to investigate the granite failure mechanisms under UHF impact as follows:

(1) Evolutionary characteristics of the maximum infrared radiation temperature can be used as a criterion for granite damage state under UHF impact: a linear increase in temperature represents elastic deformation of rock without any damage, a sharp rise in temperature represents the growth of microcracks, and the rapid fluctuation in temperature represents the extension of cracks and the generation of fracture

(2) Under test conditions, UHF impact loads can effectively damage granite specimens at amplitudes of at least 32 μm. At the optimum impact amplitude (40 μm), the UHF impact load stress propagates through the rock, driving some rock particles to vibrate against each other with an acceleration of 10^6 times and resulting in rapid fatigue damage to granite specimens

(3) The transverse fracture occurs in the upper part of the specimen subjected to confining pressure, which is quite different from the axial splitting under uniaxial UHF impact. Under the combined compression of center thermal expansion stress and confining pressure, a ring-shaped compression zone forms at the edge of the specimen, inhibiting damage to appear in this area. Eventually, fatigue cracks penetrate under shear stress to form the transverse fracture

(4) Based on the Griffith strength theory, the extension angle of fatigue cracks shifts from 60 to 30 degrees with increasing confining pressure under UHF impact

Data Availability

All data used during the study appear in the submitted article and are available from the corresponding authors upon request.

Conflicts of Interest

The authors declare that they have no conflicts of interest.

Acknowledgments

Thanks are due for the funding support of the National Natural Science Foundation of China (Project Name: Research on Mechanism of Ultrasonic Vibration Breaking Rock, Project No. 41572356) and the technical support from the Key Laboratory of Drilling and Mining Technology under Complex Conditions of Ministry of Land and Resources.

References

[1] N. Sunny, N. Mac Dowell, and N. Shah, "What is needed to deliver carbon-neutral heat using hydrogen and CCS?," *Energy & Environmental Science*, vol. 13, no. 11, pp. 4204–4224, 2020.

[2] C. Jie, H. Feiyun, X. Bin, S. Xiangchao, and L. Bo, "Drillability characteristics of formation and evaluation of bit selection for the Zhongtaishan structural strata in Sichuan Basin, China," *IOP Conference Series. Earth and Environmental Science*, vol. 570, no. 3, article 032002, 2020.

[3] J. Zhang and Y. Li, "Ultrasonic vibrations and coal permeability: laboratory experimental investigations and numerical simulations," *International Journal of Mining Science and Technology*, vol. 27, no. 2, pp. 221–228, 2017.

[4] S. Liu, Y. Cui, Y. Chen, and C. Guo, "Numerical research on rock breaking by abrasive water jet-pick under confining pressure," *International Journal of Rock Mechanics and Mining Sciences*, vol. 120, pp. 41–49, 2019.

[5] M. A. Yahaya, D. Ruan, G. Lu, and M. S. Dargusch, "Response of aluminium honeycomb sandwich panels subjected to foam projectile impact - an experimental study," *International Journal of Impact Engineering*, vol. 75, pp. 100–109, 2015.

[6] H. Gong, P. Guo, S. Chen et al., "A re-assessment of nickel-doping method in iron isotope analysis on rock samples using

multi-collector inductively coupled plasma mass spectrometry," *Acta Geochimica*, vol. 39, no. 3, pp. 355–364, 2020.

[7] Q. Li, Y. Zhai, Z. Huang, K. Chen, W. Zhang, and Y. Liang, "Research on crack cracking mechanism and damage evaluation method of granite under laser action," *Optics Communications*, vol. 506, p. 127556, 2022.

[8] G. Lu, X. Feng, Y. Li, and X. Zhang, "The microwave-induced fracturing of hard rock," *Rock Mechanics and Rock Engineering*, vol. 52, no. 9, pp. 3017–3032, 2019.

[9] Y. Wang, Q. Quan, H. Yu, D. Bai, H. Li, and Z. Deng, "Rotary-percussive ultrasonic drill: an effective subsurface penetrating tool for minor planet exploration," *IEEE Access*, vol. 6, pp. 37796–37806, 2018.

[10] M. Wiercigroch, J. Wojewoda, and A. M. Krivtsov, "Dynamics of ultrasonic percussive drilling of hard rocks," *Journal of Sound and Vibration*, vol. 280, no. 3-5, pp. 739–757, 2005.

[11] P. Harkness, "Ultrasonic rock drilling devices using longitudinal-torsional compound vibration," in *2009 IEEE International Ultrasonics Symposium*, pp. 2088–2091, Rome, Italy, 2009.

[12] A. Cardoni, P. Harkness, and M. Lucas, "Ultrasonic rock sampling using longitudinal–torsional vibrations," *Ultrasonics*, vol. 50, no. 4-5, pp. 447–452, 2010.

[13] H. Li, Y. Shen, Q. Wang, Y. Wang, D. Bai, and Z. Deng, "A piezoelectric-driven rock-drilling device for extraterrestrial subsurface exploration," *Shock and Vibration*, vol. 2018, Article ID 8368012, 12 pages, 2018.

[14] C. Zhang, D. Zhao, S. Zhang, and Y. Zhou, "Individual and combined influences of main loading parameters on granite damage development under ultrasonic vibration," *Journal of Mountain Science*, vol. 18, no. 12, pp. 3366–3379, 2021.

[15] Y. Zhou, D. Zhao, B. Li, H. Wang, Q. Tang, and Z. Zhang, "Fatigue damage mechanism and deformation behaviour of granite under ultrahigh-frequency cyclic loading conditions," *Rock Mechanics and Rock Engineering*, vol. 54, no. 9, pp. 4723–4739, 2021.

[16] Y. Zhou, Q. Tang, S. Zhang, and D. Zhao, "The mechanical properties of granite under ultrasonic vibration," *Advances in Civil Engineering*, vol. 2019, Article ID 9649165, 11 pages, 2019.

[17] S. Yin, D. Zhao, and G. Zhai, "Investigation into the characteristics of rock damage caused by ultrasonic vibration," *International Journal of Rock Mechanics and Mining Sciences*, vol. 84, pp. 159–164, 2016.

[18] Y. Zhou, D. Zhao, Q. Tang, and M. Wang, "Experimental and numerical investigation of the fatigue behaviour and crack evolution mechanism of granite under ultra-high-frequency loading," *Royal Society Open Science*, vol. 7, no. 4, article 200091, 2020.

[19] Y. Zhou, S. Yin, and D. Zhao, "Effect of static loading on rock fragmentation efficiency under ultrasonic vibration," *Geotechnical and Geological Engineering*, vol. 37, no. 4, pp. 3497–3505, 2019.

[20] D. Zhao, S. Zhang, Y. Zhao, and M. Wang, "Experimental study on damage characteristics of granite under ultrasonic vibration load based on infrared thermography," *Environmental Earth Sciences*, vol. 78, no. 14, 2019.

[21] D. Zhao, S. Zhang, and M. Wang, "Microcrack growth properties of granite under ultrasonic high-frequency excitation," *Advances in Civil Engineering*, vol. 2019, Article ID 3069029, 11 pages, 2019.

[22] Z. Wang, S. Li, L. Qiao, and J. Zhao, "Fatigue behavior of granite subjected to cyclic loading under triaxial compression condition," *Rock Mechanics and Rock Engineering*, vol. 46, no. 6, pp. 1603–1615, 2013.

[23] X. Zhu, X. Chen, and F. Dai, "Mechanical properties and acoustic emission characteristics of the bedrock of a hydropower station under cyclic triaxial loading," *Rock Mechanics and Rock Engineering*, vol. 53, no. 11, pp. 5203–5221, 2020.

[24] H. Tang, Y. Ge, L. Wang, Y. Yuan, L. Huang, and M. Sun, "Study on estimation method of rock mass discontinuity shear strength based on three-dimensional laser scanning and image technique," *Journal of Earth Science*, vol. 23, no. 6, pp. 908–913, 2012.

[25] L. Wu, S. Liu, Y. Wu, and C. Wang, "Precursors for rock fracturing and failure—part I: IRR image abnormalities," *International Journal of Rock Mechanics and Mining Sciences*, vol. 43, no. 3, pp. 473–482, 2006.

[26] L. Wu, S. Liu, Y. Wu, and C. Wang, "Precursors for rock fracturing and failure—part II: IRR T-curve abnormalities," *International Journal of Rock Mechanics and Mining Sciences*, vol. 43, no. 3, pp. 483–493, 2006.

[27] C. Wang, Z. Lu, L. Liu, X. Chuai, and H. Lu, "Predicting points of the infrared precursor for limestone failure under uniaxial compression," *International Journal of Rock Mechanics and Mining Sciences*, vol. 88, pp. 34–43, 2016.

[28] W. Li, T. Yan, S. Li, and X. Zhang, "Rock fragmentation mechanisms and an experimental study of drilling tools during high-frequency harmonic vibration," *Petroleum Science*, vol. 10, no. 2, pp. 205–211, 2013.

[29] Q. Sun, W. Zhang, L. Xue, Z. Zhang, and T. Su, "Thermal damage pattern and thresholds of granite," *Environmental Earth Sciences*, vol. 74, no. 3, pp. 2341–2349, 2015.

[30] Q. B. Zhang and J. Zhao, "A review of dynamic experimental techniques and mechanical behaviour of rock materials," *Rock Mechanics and Rock Engineering*, vol. 47, no. 4, pp. 1411–1478, 2013.

[31] K. Liu, Q. B. Zhang, G. Wu, J. C. Li, and J. Zhao, "Dynamic mechanical and fracture behaviour of sandstone under multiaxial loads using a Triaxial Hopkinson Bar," *Rock Mechanics and Rock Engineering*, vol. 52, no. 7, pp. 2175–2195, 2019.

[32] Z. Zhou, X. Cai, X. Li, W. Cao, and X. Du, "Dynamic response and energy evolution of sandstone under coupled static–dynamic compression: insights from experimental study into deep rock engineering applications," *Rock Mechanics and Rock Engineering*, vol. 53, no. 3, pp. 1305–1331, 2019.

[33] K. Peng, Z. Liu, Q. Zou, Q. Wu, and J. Zhou, "Mechanical property of granite from different buried depths under uniaxial compression and dynamic impact: an energy-based investigation," *Powder Technology*, vol. 362, pp. 729–744, 2020.